arXiv:2102.03246v2 [hep-ph] 21 Apr 2021

Combined NLO EW and QCD corrections to off-shell $t\bar{t}W$ production at the LHC

Ansgar Denner and Giovanni Pelliccioli

University of Würzburg, Institut für Theoretische Physik und Astrophysik, Emil-Hilb-Weg 22, 97074 Würzburg (Germany)

Abstract. The high luminosity that will be accumulated at the LHC will enable precise differential measurements of the hadronic production of a top–antitop-quark pair in association with a W boson. Therefore, an accurate description of this process is needed for realistic final states. In this work we combine for the first time the NLO QCD and electroweak corrections to the full off-shell $t\bar{t}W^+$ production at the LHC in the three-charged-lepton channel, including all spin correlations, non-resonant effects, and interferences. To this end, we have computed the NLO electroweak radiative corrections to the leading QCD order as well as the NLO QCD corrections to both the QCD and the electroweak leading orders.

1 Introduction

The hadronic production of top-antitop pairs in association with a W boson is an interesting process to investigate at the Large Hadron Collider (LHC), as it represents an important probe of the Standard Model (SM) as well as a window to new physics.

This process is one of the heaviest signatures measurable at the LHC. It gives access to the top-quark coupling to weak bosons and to possible deviations from its SM value [1–3]. Due to the absence of a neutral initial state at a lower perturbative order than next-to-next-to-leading order (NNLO) in QCD, it is also expected to improve substantially the sensitivity to the $t\bar{t}$ charge asymmetry [4]. Polarization observables and asymmetries in $t\bar{t}W^\pm$ production are capable of enhancing the sensitivity to beyond-the-SM (BSM) interactions featuring a chiral structure different from the one of the SM [4, 5]. The hadro-production of $t\bar{t}W^\pm$ is in general well suited to directly search for BSM physics, in particular supersymmetry [6, 7], supergravity [8], technicolour [9], vector-like quarks [10], Majorana neutrinos [11] and modified Higgs sectors [12–14]. Beyond its own importance in LHC searches, the $t\bar{t}W$ production is a relevant background to $t\bar{t}H$ production [15].

The ATLAS and CMS collaborations have measured and investigated $t\bar{t}W^\pm$ production at Run 1 [16, 17] and Run 2 [18–21] of the LHC. This signature has been included as a background in the recent experimental analyses for $t\bar{t}H$ production [22–25].

The most recent experimental results based on Run 2 show a tension between data and theory predictions in the $t\bar{t}W$ modelling both in direct measurements [19, 20] and in the context of the search for $t\bar{t}$ associated production with a Higgs boson [24, 25]. While the theoretical community has invested a noticeable effort to address this tension, so far no explanation emerged that is capable to fill the gap between the SM predictions and the data.

An improved modelling of the $t\bar{t}W^\pm$ process is required to allow for the comparison of SM predictions with future LHC data, particularly those that will be accumulated during the high-luminosity run. The increased statistics will enable not only more precise measurements of $t\bar{t}W^\pm$ cross-sections, but also measurements of differential distributions and in different decay channels. This target can only be achieved if the theoretical description of realistic final states embedding the $t\bar{t}W$ resonance structure is available.

Many theoretical predictions for $t\bar{t}W^\pm$ hadro-production are available in the literature. The first next-to-leading order (NLO) QCD calculation for TeV-scale colliders was performed in a spin-correlated narrow-width approximation for the semi-leptonic decay channel [26]. The matching of NLO QCD predictions to a parton shower was first tackled for the same decay channel in Ref. [27]. A number of calculations for $t\bar{t}W^\pm$ inclusive production (on-shell top/antitop quarks and W boson) have been carried out, targeting charge asymmetries [4], the impact of $t\bar{t}W^\pm$ on the associated production of $t\bar{t}$ pairs with a Higgs boson [15] at NLO QCD, and the effects of subleading NLO QCD and electroweak (EW) corrections [28–30]. Soft-gluon resummation up to next-to-next-to-leading logarithmic accuracy [31–35] and multi-jet merging [36] have also been investigated. NLO QCD corrections to the EW leading order (LO) have been computed in the narrow-width approximation (NWA), accounting for complete spin correlations and including parton-shower effects [37, 38]. Very recently a comparison of different fixed-order Monte Carlo generators matched to parton showers has been performed for inclusive $t\bar{t}W^\pm$, with a focus on the

two-charged lepton signature (in the NWA) [38]. The first studies that aim at the off-shell modelling of $t\bar{t}W$ production concern the full NLO QCD corrections in the three-charged-lepton channel [5, 39, 40].

The calculation of subleading NLO corrections has been performed for inclusive production [28–30, 37, 38], but is still missing for realistic final states. Our present work targets the complete fixed-order description of the off-shell $t\bar{t}W$ production, combining the NLO QCD and EW corrections that have a sizeable impact at the LHC@13TeV.

This paper is organized as follows. In Section 2.1 we describe the process under investigation, providing details on various NLO corrections that are presented. In Sections 2.2 and 2.3 we provide the SM input parameters and the selection cuts used for numerical simulations, respectively. The integrated results at LO and NLO are presented in Section 3.1, while in Section 3.2 a number of differential distributions are described, focusing on the relative impact of various NLO corrections to the LO predictions. In Section 4 we draw our conclusions.

2 Details of the calculation

2.1 Description of the process

We consider the process

$$\mathrm{pp} \to \mathrm{e}^+\nu_\mathrm{e}\tau^+\nu_\tau\mu^-\bar{\nu}_\mu\,\mathrm{b}\,\bar{\mathrm{b}} + X\,, \tag{1}$$

which receives contributions only from quark-induced partonic channels at LO. Gluon–quark and photon–quark channels open up at NLO, while the pure gluonic channel enters only at NNLO in QCD.

Although we consider the final state with three charged leptons with different flavours, the corresponding results for the case of identical positively-charged leptons can be estimated by multiplying our results by a factor 1/2, up to interference contributions, which are expected to be small.

In this work we focus on the production of $t\bar{t}$ pairs in association with a W^+ boson, but the calculation of the charge-conjugate process ($t\bar{t}W^-$) can be performed with the same techniques and no additional conceptual issues.

At LO, the largest contribution is given by the QCD-mediated process of order $\mathcal{O}(\alpha_\mathrm{s}^2\alpha^6)$ (labelled $\mathrm{LO_{QCD}}$), which always embeds a gluon s-channel propagator if no quark-family mixing is assumed (diagonal quark-mixing matrix with unit entries). The tree-level EW contribution of order $\mathcal{O}(\alpha^8)$ (labelled $\mathrm{LO_{EW}}$), despite being characterized by many more diagram topologies, is expected to give a cross-section that is roughly 1% of the $\mathrm{LO_{QCD}}$ one owing to the ratio of EW and strong coupling constants. The interference contribution, formally of order $\mathcal{O}(\alpha_\mathrm{s}\alpha^7)$, is identically zero due to colour algebra. In Fig. 1 we show sample diagrams for the QCD-mediated and purely-EW process. Note that the diagrams with a resonant top–antitop-quark pair are present also in EW tree-level contributions.

At NLO, the $t\bar{t}W$ process receives contributions from four different perturbative orders, as depicted in Fig. 2.

The corrections that have the largest impact on the NLO cross-section are of order $\mathcal{O}(\alpha_\mathrm{s}^3\alpha^6)$, which are pure QCD corrections to $\mathrm{LO_{QCD}}$. Following the notation of Refs. [29, 30], we label this perturbative order as $\mathrm{NLO_1}$. These corrections have recently been computed for the full off-shell process [39, 40]. This perturbative order shows a typical NLO QCD behaviour in the scale dependence, and the NLO relative corrections to $\mathrm{LO_{QCD}}$ are at the 10–20% level, depending on the choice of the renormalization and factorization scale [40].

The $\mathrm{NLO_2}$ corrections are known only for on-shell top–antitop quarks and for an on-shell W boson [28–30]. They are expected to give a negative contribution of about 4.5% of the inclusive LO cross-section.

In the off-shell calculation, as well as in the on-shell one, the $\mathrm{NLO_2}$ order receives contributions not only from the EW corrections to $\mathrm{LO_{QCD}}$, but also from the QCD corrections to the LO interference, although at Born-level the $\mathcal{O}(\alpha_\mathrm{s}\alpha^7)$ contribution vanishes.

Sample contributions to the virtual corrections at order $\mathcal{O}(\alpha_\mathrm{s}^2\alpha^7)$ are shown in Fig. 3. The diagram on the left involves one-loop amplitudes of order $\mathcal{O}(g_\mathrm{s}^4 g^6)$ interfered with tree-level EW amplitudes of order $\mathcal{O}(g^8)$ and is obviously a QCD correction to the LO interference. The diagram on the right involves one-loop amplitudes of order $\mathcal{O}(g_\mathrm{s}^2 g^8)$ interfered with tree-level QCD amplitudes of order $\mathcal{O}(g_\mathrm{s}^2 g^6)$ and could be naïvely classified as an EW correction to $\mathrm{LO_{QCD}}$. However, it can also be regarded as contributing to the QCD corrections to the LO interference. In fact, the IR singularities of this contribution are partially cancelled by the real photonic corrections to $\mathrm{LO_{QCD}}$ and partially by the real gluonic corrections to the LO interference. Diagrams with weakly-interacting particles in the loops are more demanding from the computational point of view, as the corresponding one-loop amplitudes include up to 10-point functions, while the latter ones feature at most 7-point functions. A selection of one-loop diagrams which contribute at this perturbative order are shown in Fig. 4.

The real-radiation contributions to $\mathrm{NLO_2}$ corrections are computationally demanding due to the large multiplicity of electrically charged final-state particles. In contrast to the virtual ones, the real $\mathrm{NLO_2}$ corrections can be uniquely classified into two types: the NLO EW corrections to the $\mathrm{LO_{QCD}}$ process, which involve a real photon (see Fig. 5 left for an example), and the NLO QCD corrections to the LO interference, which involve a real gluon (see Fig. 5 right for an example). In the first class of contributions, the photon can be either in the final or in the initial state. The processes with a photon in the final state are characterized by many singular regions, as the photon can become soft or collinear to any of the seven charged external particles. This results in a large number of subtraction counterterms that are required to ensure a stable calculation of the NLO cross-section. The real processes with a photon in the initial state possess a smaller number of singular phase-space regions and are suppressed due to the small luminosity of photons in the proton. For on-shell production, the contribution of the photon-induced channels to the leading-order cross-section is at the sub-percent level [28]. The QCD corrections to the

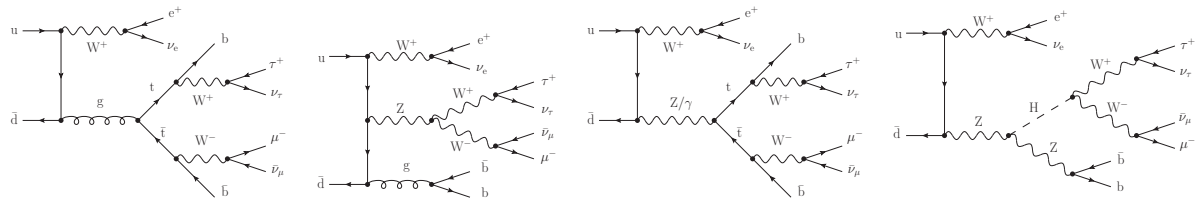

Fig. 1. Sample diagrams contributing to $\mathrm{LO_{QCD}}$ (left) and to $\mathrm{LO_{EW}}$ (right) cross-sections for off-shell $t\bar{t}W^+$ production in the three-charged-lepton channel.

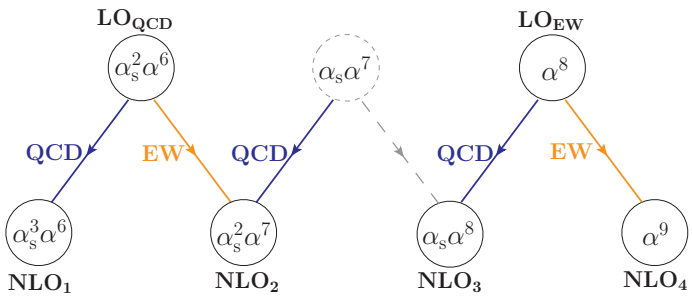

Fig. 2. Contributing perturbative orders at LO and NLO for $t\bar{t}W$ hadro-production in the three-charged-lepton channel.

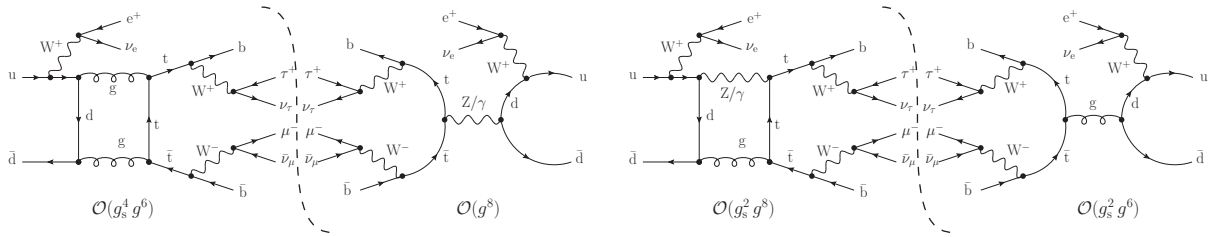

Fig. 3. Sample contributions to the virtual corrections at order $\mathcal{O}(\alpha_s^2\alpha^7)$ for off-shell $t\bar{t}W$ production in the three-charged-lepton channel: QCD corrections to the LO interference (left) and a contribution that cannot be uniquely attributed to either the QCD corrections to the LO interference or the EW corrections to the $\mathrm{LO_{QCD}}$ (right).

LO interference are non-vanishing only if the radiated gluon is emitted by an initial-state light quark and absorbed by a final-state b quark or top quark (or the other way around). A sample contribution is shown in Fig. 5 right. These corrections, although necessary to account for all $\mathcal{O}(\alpha_s^2\alpha^7)$ contributions, turn out to be very small, as detailed in Section 3.

To sum up, the full set of real partonic channels that contribute to the $\mathrm{NLO_2}$ corrections is

$$\left.\begin{array}{l} u\,\bar{d} \to \mathrm{e}^+\nu_\mathrm{e}\,\mu^-\bar{\nu}_\mu\,\tau^+\nu_\tau\,\mathrm{b}\,\bar{\mathrm{b}}\,\gamma \\ \gamma\,u \to \mathrm{e}^+\nu_\mathrm{e}\,\mu^-\bar{\nu}_\mu\,\tau^+\nu_\tau\,\mathrm{b}\,\bar{\mathrm{b}}\,d \\ \gamma\,\bar{d} \to \mathrm{e}^+\nu_\mathrm{e}\,\mu^-\bar{\nu}_\mu\,\tau^+\nu_\tau\,\mathrm{b}\,\bar{\mathrm{b}}\,\bar{u} \end{array}\right\}\text{EW corr. to } \mathrm{LO_{QCD}}$$

and

$$\left.\begin{array}{l} u\,\bar{d} \to \mathrm{e}^+\nu_\mathrm{e}\,\mu^-\bar{\nu}_\mu\,\tau^+\nu_\tau\,\mathrm{b}\,\bar{\mathrm{b}}\,\mathrm{g} \\ \mathrm{g}\,u \to \mathrm{e}^+\nu_\mathrm{e}\,\mu^-\bar{\nu}_\mu\,\tau^+\nu_\tau\,\mathrm{b}\,\bar{\mathrm{b}}\,d \\ \mathrm{g}\,\bar{d} \to \mathrm{e}^+\nu_\mathrm{e}\,\mu^-\bar{\nu}_\mu\,\tau^+\nu_\tau\,\mathrm{b}\,\bar{\mathrm{b}}\,\bar{u} \end{array}\right\}\text{QCD corr. to LO int.,}$$

where u and d stand for up-type and down-type quarks, respectively (of the first and second generation).

The vanishing LO interference implies that the corresponding EW corrections vanish as well, since additional EW propagators (virtual contributions) and radiated photons (real contributions) do not modify the LO colour structure. Therefore, the only NLO corrections that contribute at order $\mathcal{O}(\alpha_s\alpha^8)$ are genuine QCD corrections to the $\mathrm{LO_{EW}}$ cross-section. This order is labelled as $\mathrm{NLO_3}$ in Fig. 2. By simply counting the powers of α_s the $\mathrm{NLO_3}$ corrections are expected to give a smaller contribution than the $\mathrm{NLO_2}$ ones. However, at the inclusive level [29] and in the narrow-width approximation [37, 38], they are noticeably larger than the $\mathrm{NLO_2}$ ones. This results from the fact that this perturbative order is dominated by hard real radiation diagrams in the gluon-quark partonic channel that embed the tW scattering process [1]. Sample diagrams are shown in Fig. 6. Thanks to the genuine QCD nature of the $\mathrm{NLO_3}$ corrections, it is possible to match them to a QCD parton shower with no subtleties due to EW corrections, as it has been done in Refs. [37, 38].

The last NLO perturbative order, $\mathcal{O}(\alpha^9)$, is furnished by the EW corrections to the $\mathrm{LO_{EW}}$ process. It has been shown at the inclusive level that such contributions are at the sub-permille level [30], as expected by naïve power counting. Even with a substantially larger data set than the one of Run 2 (*i.e.* 3000 fb^{-1} at the high-luminosity LHC) these EW effects are out of reach in a realistic

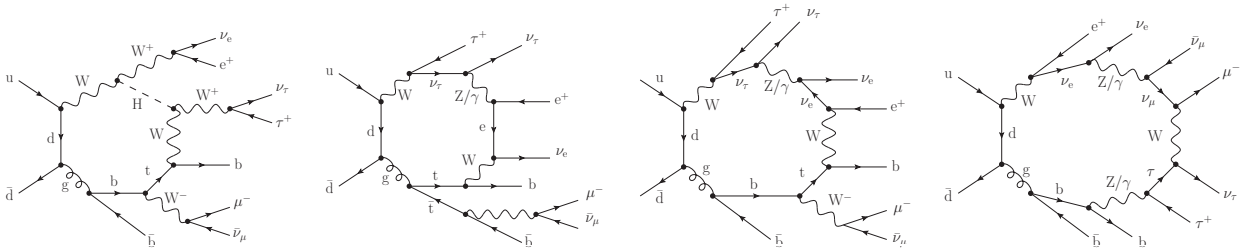

Fig. 4. One-loop diagrams of order $\mathcal{O}(g_s^2 g^8)$ contributing to the EW virtual corrections ($\mathrm{NLO_2}$) to off-shell $\mathrm{t\bar{t}W}$ production in the three-charged-lepton channel. From left to right: sample diagrams involving 7-, 8-, 9- and 10-point functions.

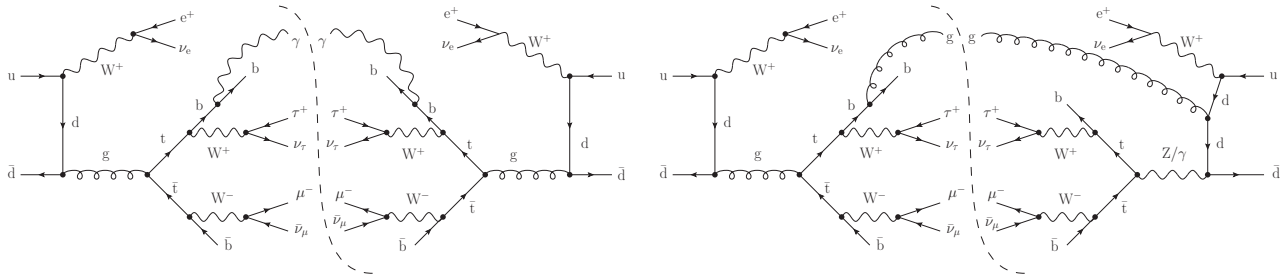

Fig. 5. Sample contribution to the real corrections at order $\mathcal{O}(\alpha_s^2\alpha^7)$ for $\mathrm{t\bar{t}W}$ production in the three-charged-lepton channel: photonic corrections to $\mathrm{LO_{QCD}}$(left) and gluonic corrections to the LO interference (right).

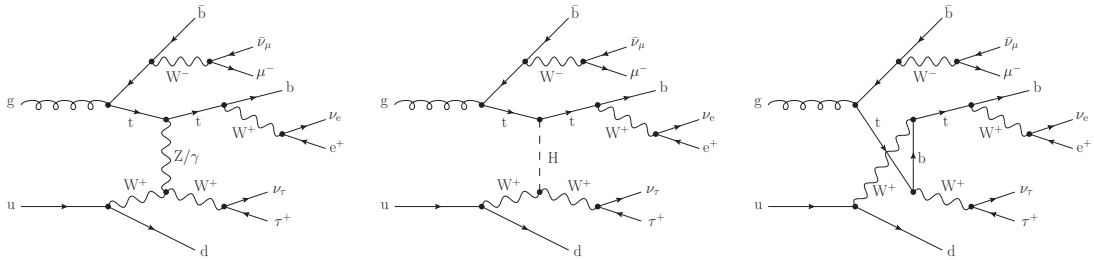

Fig. 6. Sample diagrams for the partonic channel $\mathrm{gu} \to \mathrm{b\,\bar{b}\,e^+\nu_e\tau^+\nu_\tau\mu^-\bar{\nu}_\mu d}$ that contain $\mathrm{tW^+}$ scattering as a subprocess and contribute to $\mathrm{NLO_3}$ corrections to $\mathrm{t\bar{t}W}$ production in the three-charged-lepton channel.

fiducial region. Therefore, we are not providing results for this order.

In the following we focus on the first three NLO perturbative orders. Tree-level and one-loop SM amplitudes are computed with the Recola matrix-element provider [41, 42]. For the tensor reduction and evaluation of loop integrals we use the Collier library [43]. The multi-channel Monte Carlo integration is performed with MoCaNLO, a generator that has already been used to compute the NLO QCD corrections to $\mathrm{t\bar{t}W}$ [40] and the NLO EW corrections to several LHC processes involving top quarks [44, 45]. The subtraction of infrared and collinear singularities is carried out using the dipole formalism of Refs. [46–48] both for QCD and for EW corrections. The initial-state collinear singularities are absorbed in the parton distribution functions (PDFs) in the $\overline{\mathrm{MS}}$ factorization scheme.

2.2 Input parameters

We consider proton–proton collisions at a centre-of-mass energy of 13 TeV. We neglect flavour mixing in the quark sector and use a unit quark-mixing matrix. The three charged leptons that we consider in the final state are massless and characterized by three different flavours. The on-shell masses and widths of weak bosons are set to the following values [49],

$$M_\mathrm{W}^\mathrm{OS} = 80.379\,\mathrm{GeV}, \qquad \Gamma_\mathrm{W}^\mathrm{OS} = 2.085\,\mathrm{GeV}\,,$$
$$M_\mathrm{Z}^\mathrm{OS} = 91.1876\,\mathrm{GeV}, \qquad \Gamma_\mathrm{Z}^\mathrm{OS} = 2.4952\,\mathrm{GeV}\,, \tag{2}$$

and then translated into their pole values [50] that enter the Monte Carlo simulations. The Higgs-boson mass and width are fixed, following Ref. [49], to

$$M_\mathrm{H} = 125\,\mathrm{GeV}, \qquad \Gamma_\mathrm{H} = 0.00407\,\mathrm{GeV}\,. \tag{3}$$

We have computed the LO top-quark width according to Ref. [51], using the pole values for the W-boson mass and width. The NLO top-quark width is obtained applying the NLO QCD and EW correction factors of Ref. [52] to the LO width. The numerical values read

$$m_\mathrm{t} = 173.0\,\mathrm{GeV}\,,$$
$$\Gamma_\mathrm{t}^\mathrm{LO} = 1.4437\,\mathrm{GeV}\,, \quad \Gamma_\mathrm{t}^\mathrm{NLO} = 1.3636\,\mathrm{GeV}\,. \tag{4}$$

The top-quark width is kept fixed when performing variations of the factorization and renormalization scales. The EW coupling is treated in the G_μ scheme [53],

$$\alpha = \frac{\sqrt{2}}{\pi} G_\mu M_{\mathrm{W}}^2 \left[1 - \frac{M_{\mathrm{W}}^2}{M_{\mathrm{Z}}^2}\right], \tag{5}$$

where $G_\mu = 1.16638 \cdot 10^{-5}\,\mathrm{GeV}^{-2}$ is the Fermi constant. The masses of weak bosons and of the top quark, and therefore also the EW mixing angle, are treated in the complex-mass scheme [53–56].

Both for LO and NLO predictions, we employ NNPDF_3.1_luxQED PDFs [57]. Using these PDFs, the photon contribution is properly accounted for in the evolution. The evaluation of PDFs and the running of the strong coupling are obtained via the LHAPDF6 interface [58]. The employed PDF set uses $\alpha_{\mathrm{s}}(M_{\mathrm{Z}}) = 0.118$ and one QCD loop in the calculation of the α_{s} evolution.

2.3 Selection cuts

Coloured partons with $|\eta| < 5$ are clustered into jets by means of the anti-k_t algorithm [59] with resolution radius $R = 0.4$. The same algorithm but with $R = 0.1$ is applied to cluster photons into charged particles.

We choose cuts that mimic the fiducial selections applied by ATLAS in Ref. [20] and that have already been used for the study of NLO QCD corrections to the same final state [40]. We select events with exactly two b jets (assuming perfect b-tagging efficiency) that are required to satisfy

$$p_{\mathrm{T,b}} > 25\,\mathrm{GeV}\,, \quad |\eta_{\mathrm{b}}| < 2.5\,. \tag{6}$$

Furthermore, we ask for three charged leptons that fulfil standard acceptance and isolation cuts,

$$p_{\mathrm{T},\ell} > 27\,\mathrm{GeV}\,, \quad |\eta_\ell| < 2.5\,, \quad \Delta R_{\ell\mathrm{b}} > 0.4\,, \tag{7}$$

where the R distance is defined as the sum in quadrature of the azimuthal and rapidity separations,

$$\Delta R_{ij} = \sqrt{\Delta\phi_{ij}^2 + \Delta y_{ij}^2}\,. \tag{8}$$

We do not constrain the missing transverse momentum and do not apply any veto to additional light jets.

3 Results

For the factorization and renormalization scale ($\mu_{\mathrm{F}} = \mu_{\mathrm{R}}$), we consider two different dynamical choices that have proved to behave better than a fixed scale [39, 40]. The first one, introduced in Ref. [39], depends on the transverse-momentum content of the final-state particles, regardless of the top–antitop resonances,[1]

$$\mu_0^{(\mathrm{c})} = \frac{H_{\mathrm{T}}}{3} = \frac{p_{\mathrm{T,miss}} + \sum_{i=\mathrm{b},\ell} p_{\mathrm{T},i}}{3}\,. \tag{9}$$

[1] We use the same notation for the scales as in Ref. [40].

The second dynamical choice, already used in Ref. [40], is based on the transverse masses of the top and antitop quarks. Due to the ambiguity in choosing the $\ell^+\nu_\ell$ pair that results from the top quark, we pick the pair of leptons that when combined with the bottom quark forms an invariant mass closest to the top-quark mass. We consider two different central-scales based on this dynamical choice,

$$\mu_0^{(\mathrm{d})} = \sqrt{\sqrt{m_{\mathrm{t}}^2 + p_{\mathrm{T,t}}^2}\sqrt{m_{\mathrm{t}}^2 + p_{\mathrm{T},\bar{\mathrm{t}}}^2}}\,, \qquad \mu_0^{(\mathrm{e})} = \frac{\mu_0^{(\mathrm{d})}}{2}\,. \tag{10}$$

The scale-dependence study performed in Ref. [40] shows that using $\mu_0^{(\mathrm{e})}$ as a central scale reduces the scale dependence based on the conventional 7-point scale variation and gives smaller QCD corrections than using $\mu_0^{(\mathrm{d})}$. Therefore, the choice $\mu_0^{(\mathrm{e})}$ is preferable for the study of the impact of NLO_2 and NLO_3 corrections, which is the focus of this work.

The scale uncertainties shown in the following results are based on 7-point scale variations, *i.e.* rescaling the central factorization and renormalization scale by the factors

$$(0.5, 0.5)\,, (1, 0.5)\,, (0.5, 1)\,, (1, 1)\,, (1, 2)\,, (2, 1)\,, (2, 2)\,,$$

while keeping the NLO QCD top-quark width fixed.

In the following we present the results combining NLO corrections with the so-called *additive* approach,

$$\sigma_{\mathrm{LO+NLO}} = \sigma_{\mathrm{LO_{QCD}}} + \sigma_{\mathrm{NLO_1}} + \sigma_{\mathrm{NLO_2}} + \sigma_{\mathrm{LO_{EW}}} + \sigma_{\mathrm{NLO_3}}. \tag{11}$$

This approach is exact at the order of truncation of the perturbative expansion. Furthermore, it represents a natural choice for our process, as the combination involves NLO corrections to two different leading orders that do not interfere.

3.1 Integrated cross-sections

In Table 1, we present the integrated cross-sections in the fiducial region defined in Section 2.3.

The leading corrections to the $\mathrm{LO_{QCD}}$ cross-section are expected to come from the corresponding pure QCD radiative corrections ($\mathrm{NLO_1}$). Their inclusion has been proved to decrease the theoretical uncertainty due to scale variations and to stabilize the perturbative convergence for this process. Nonetheless, their impact depends on the choice of the scale, as already pointed out both in inclusive [28, 29] and off-shell [39, 40] computations. In fact, with the resonance-blind dynamical choice $\mu_0^{(\mathrm{c})}$, the $\mathrm{NLO_1}$ corrections give a 6.6% enhancement to the $\mathrm{LO_{QCD}}$ cross-section, with the resonance-aware choices, $\mu_0^{(\mathrm{d})}$ and $\mu_0^{(\mathrm{e})}$, they give a 18% and a 0.4% correction, respectively. Note that, at variance with Ref. [40] in this paper we compute both LO and NLO predictions with the NLO top-quark width, which gives roughly a 12% enhancement to the LO cross-section.

	$\mu_0^{(c)}$		$\mu_0^{(d)}$		$\mu_0^{(e)}$	
perturbative order	σ (fb)	ratio	σ (fb)	ratio	σ (fb)	ratio
$\mathrm{LO_{QCD}}$ ($\alpha_s^2\alpha^6$)	$0.2218(1)^{+25.3\%}_{-18.8\%}$	1	$0.1948(1)^{+23.9\%}_{-18.1\%}$	1	$0.2414(1)^{+26.2\%}_{-19.3\%}$	1
$\mathrm{LO_{EW}}$ (α^8)	$0.002164(1)^{+3.7\%}_{-3.6\%}$	0.010	$0.002122(1)^{+3.7\%}_{-3.6\%}$	0.011	$0.002201(1)^{+3.7\%}_{-3.6\%}$	0.009
$\mathrm{NLO_1}$ ($\alpha_s^3\alpha^6$)	0.0147(6)	0.066	0.0349(6)	0.179	0.0009(7)	0.004
$\mathrm{NLO_2}$ ($\alpha_s^2\alpha^7$)	-0.0122(3)	-0.055	-0.0106(3)	-0.054	-0.0134(4)	-0.056
$\mathrm{NLO_3}$ ($\alpha_s\alpha^8$)	0.0293(1)	0.131	0.0263(1)	0.135	0.0320(1)	0.133
$\mathrm{LO_{QCD}}$+$\mathrm{NLO_1}$	$0.2365(6)^{+2.9\%}_{-6.0\%}$	1.066	$0.2297(6)^{+5.5\%}_{-7.3\%}$	1.179	$0.2423(7)^{+3.5\%}_{-5.2\%}$	1.004
$\mathrm{LO_{QCD}}$+$\mathrm{NLO_2}$	$0.2094(3)^{+25.0\%}_{-18.7\%}$	0.945	$0.1840(3)^{+23.8\%}_{-17.9\%}$	0.946	$0.2277(4)^{+25.9\%}_{-19.2\%}$	0.944
$\mathrm{LO_{EW}}$+$\mathrm{NLO_3}$	$0.03142(4)^{+22.2\%}_{-16.8\%}$	0.141	$0.02843(6)^{+20.5\%}_{-15.6\%}$	0.146	$0.03425(7)^{+22.8\%}_{-17.0\%}$	0.142
LO+NLO	$0.2554(7)^{+4.0\%}_{-6.5\%}$	1.151	$0.2473(7)^{+6.3\%}_{-7.6\%}$	1.270	$0.2628(9)^{+4.3\%}_{-5.9\%}$	1.089

Table 1. LO cross-sections and NLO corrections (in fb) in the fiducial setup, for three different dynamical-scale choices. Numerical errors (in parentheses) are shown. Ratios are relative to the $\mathrm{LO_{QCD}}$ cross-section. The scale uncertainties from 7-point scale variations (in percentage) are listed for LO and NLO cross-sections. The result in the last row is the sum of all LO cross-sections and NLO corrections, namely $\mathrm{LO_{QCD}} + \mathrm{LO_{EW}} + \mathrm{NLO_1} + \mathrm{NLO_2} + \mathrm{NLO_3}$.

The $\mathrm{NLO_2}$ corrections are negative and amount to about -5.5% of the $\mathrm{LO_{QCD}}$ cross-section for all scale choices. Such supposedly subleading corrections have a sizeable impact on the fiducial NLO cross-section, and this is likely due to large EW Sudakov logarithms enhancing the cross-section in the high-energy regime [60]. This is supported by the fact that the average partonic centre-of-mass energy and H_T are quite high, 850 GeV and 520 GeV, respectively. A crude estimate of the Sudakov logarithms gives a result which is of the same order of magnitude as the full $\mathrm{NLO_2}$ corrections we have obtained for this process.

The impact of QCD corrections that can be uniquely attributed to the LO interference is very small, both for real and for virtual corrections, accounting respectively for 5% and for less than 1% of the total $\mathrm{NLO_2}$ result.

At $\mathcal{O}(\alpha_s^2\alpha^7)$, we have also included the contribution from photon-initiated partonic channels, which are positive and account for about 0.1% of the LO QCD cross-section. As already observed at the inclusive level [28], this contribution is very small and its effect will be hardly visible even at the high-luminosity run of LHC (they will yield about 1 event for $\sqrt{s} = 13$ TeV and $\mathcal{L} = 3000\,\mathrm{fb}^{-1}$).

In inclusive calculations with on-shell top–antitop quarks, the $\mathrm{NLO_2}$ corrections were found to give a -4.5% contribution to the inclusive production cross-section [28, 30]. In order to compare our results with those of Ref. [30], we have performed a full off-shell calculation in a very inclusive setup, and divided by the branching ratios for the decays of the top and antitop quarks and of the W boson. The setup is the same as the one of Ref. [30], up to a few unavoidable differences:

- we use finite top-quark and W widths (same values as those of Section 2.2) and we include Higgs-boson contributions;
- we apply a minimum invariant-mass cut of 5 GeV to the bb system to protect from infrared singularities and we cluster photons into charged particles with isolation radius $R = 0.1$;
- we employ the same dynamical scale as in Ref. [30], but using the kinematics after photon recombination and choosing the top-quark candidate with the same invariant-mass prescription as for the calculation of the scales $\mu_0^{(d)}$ and $\mu_0^{(e)}$.

The obtained inclusive cross-sections,

$$\sigma_{\mathrm{LO_{QCD}}} = 262^{+23.7\%}_{-18.1\%}\,\mathrm{fb},$$
$$\sigma_{\mathrm{LO_{QCD}+NLO_2}} = 254^{+23.4\%}_{-17.8\%}\,\mathrm{fb}\,, \qquad (12)$$

exhibit $\mathrm{NLO_2}$ corrections of -3% of $\mathrm{LO_{QCD}}$, which is not far from the -4.5% of Refs. [28, 30]. The remaining discrepancy should be due to both the additional cuts we have applied and the non-resonant effects that are included in our full calculation, while being absent in on-shell calculations. The comparison of results in the fiducial and the inclusive setup reveals that the $\mathrm{NLO_2}$ corrections are more sizeable for realistic final states and in the presence of reasonable fiducial cuts.

Coming back to our default fiducial setup (see Section 2.3), the $\mathrm{NLO_3}$ perturbative order is dominated by the real radiation in the ug partonic channel, owing to a PDF enhancement and the tW scattering embedded in this channel. These real corrections account for 85% of the $\mathrm{NLO_3}$ corrections, and are one order of magnitude larger than the corresponding leading order $\mathrm{LO_{EW}}$. The total $\mathrm{NLO_3}$ corrections amount to 13% of the $\mathrm{LO_{QCD}}$ cross-section, almost independently of the scale choice. This confirms the 12% effect obtained in the case of on-shell top and antitop quarks [30].

It is worth stressing that the inclusion of $\mathrm{NLO_2}$ and $\mathrm{NLO_3}$ corrections gives a noticeable effect to the $t\bar{t}W$ cross-section. Therefore such corrections must definitely be accounted for in experimental analyses. Furthermore,

their relative contribution to the LO result is rather independent of the scale choice, while the NLO_1 corrections are much more scale dependent.

As a last comment of this section, we point out that the scale uncertainty of the combined LO+NLO cross-section is driven by the NLO_1 corrections which reduce the $\mathrm{LO}_{\mathrm{QCD}}$ uncertainty roughly from 20% to 5%. Due to their EW nature, the NLO_2 corrections do not diminish the scale uncertainty of the corresponding leading order ($\mathrm{LO}_{\mathrm{QCD}}$). The NLO_3 corrections exceed the corresponding pure EW LO process and, thus, imply a LO-like scale dependence for $\mathrm{LO}_{\mathrm{EW}}+\mathrm{NLO}_3$.

So far, we have focused on the relative contributions of various NLO corrections to the fiducial $t\bar{t}W$ cross-section. However, the interplay among different corrections can be rather different for more exclusive observables. Therefore, it is essential to study differential distributions.

3.2 Distributions

In the following we present a number of relevant distributions focusing on the impact of the various NLO corrections relative to the $\mathrm{LO}_{\mathrm{QCD}}$ cross-sections. Since in most of the LHC experimental analyses the theoretical predictions are NLO QCD accurate, we also comment on the distortion of NLO QCD distribution shapes ($\mathrm{LO}_{\mathrm{QCD}} + \mathrm{NLO}_1$ in our notation) due to the inclusion of NLO_2 and NLO_3 corrections. We choose to present all differential distributions with the $\mu_0^{(\mathrm{e})}$ scale.[2] The shown scale uncertainties are based on the predictions for $\mathrm{LO}_{\mathrm{QCD}} + \mathrm{NLO}_1$, normalized to predictions at the central scale in the relative plots.

We start by presenting transverse-momentum distributions in Figs. 7–8.

In Fig. 7(a) we consider the distribution in the transverse momentum of the positron, which is precisely measurable at the LHC. Since we also include EW corrections (NLO_2), the positron is understood as dressed (a radiated photon could be clustered into the positron). The distribution peaks around 50 GeV, where the relative impact of QCD and EW corrections follows straight the integrated results. Relative to the $\mathrm{LO}_{\mathrm{QCD}}$, all three radiative corrections drop in a monotonic manner. Nonetheless, the decrease of NLO_3 corrections is very mild (14% below 50 GeV, 10% at 380 GeV), while the NLO_1 and NLO_2 corrections decrease steeper: the former become negative around 80 GeV and give -9% at 380 GeV, the latter become lower than -10% already at moderate $p_{\mathrm{T,e^+}}$ (200 GeV). The behaviour of EW corrections in the tails of this distribution is likely driven by the impact of Sudakov logarithms, which become large at high p_{T}.

The same behaviour of the NLO_2 and NLO_3 corrections characterizes also the distribution in the transverse momentum of the antitop quark, shown in Fig. 7(b). The antitop momentum is computed as the sum of the momenta of the muon, its corresponding antineutrino, and the antibottom quark. This is not observable at the LHC, but its analysis is useful to compare the full off-shell calculation with the on-shell ones. The negative growth of the NLO_2 corrections behaves very similarly in the inclusive calculations, as can be seen for example in Ref. [28] (figure 5 therein). This confirms that for sufficiently inclusive variables the NLO EW effects are dominated by contributions with resonant top and antitop quarks. The NLO_1 corrections increase by roughly 25% in the considered spectrum.

In both transverse-momentum distributions of Fig. 7, the inclusion of subleading NLO corrections ($\mathrm{NLO}_2, \mathrm{NLO}_3$) gives a decreasing effect towards large transverse momenta to the NLO QCD cross-section. In fact, the ratio between the combined LO + NLO cross-section and the $\mathrm{LO}_{\mathrm{QCD}} + \mathrm{NLO}_1$ one ranges between 1.10 and 1.15 for small transverse momenta and drops below 1 already at moderate transverse momenta. We have checked numerically that this conclusion can be drawn also for other scale choices ($\mu_0^{(\mathrm{c})}$, $\mu_0^{(\mathrm{d})}$), confirming the almost scale-independent impact of the NLO_2 and NLO_3 corrections.

In Fig. 8 we consider the distributions in the transverse momentum of the $t\bar{t}$ and the $b\bar{b}$ system. The former is not measurable at the LHC but can be reconstructed from Monte Carlo truth, choosing the positively-charged lepton–neutrino pair that best reconstructs the top-quark mass when combined with the momentum of the bottom quark. The latter variable is directly observable at the LHC.

The NLO_1 corrections to the $t\bar{t}$ transverse-momentum distribution [Fig. 8(a)] have already been investigated in Ref. [40]: these QCD corrections grow monotonically and become dramatically large and positive at high $p_{\mathrm{T},t\bar{t}}$. Note that at LO this variable coincides with the p_{T} of the recoiling W^+ boson, and therefore is sensitive to the real QCD radiation which is not clustered into b jets (and that cannot be clustered to the W^+-boson decay products). The NLO_1 corrections receive a sizeable contribution by the $gq/g\bar{q}$ partonic channels, which are enhanced by the gluon PDF. In contrast, the NLO_2 ones feature a typical NLO EW behaviour in the tail of the distribution, giving a negative and monotonically decreasing correction to the LO cross-section. Differently from the QCD corrections, the additional photon can be clustered into any of the external charged particles, thus also into the decay products of the recoiling W boson. Furthermore, the cross-section is not enhanced by the $\gamma q/\gamma\bar{q}$ partonic channels due to the very small photon luminosity in the proton. The NLO_3 contribution is positive in the whole analyzed spectrum, and increases from 6% (below 50 GeV) to a maximum of 25% around $p_{\mathrm{T},t\bar{t}} = 2m_{\mathrm{t}}$, then it slowly decreases in the large-p_{T} region. Relative to the $\mathrm{LO}_{\mathrm{QCD}} + \mathrm{NLO}_1$ result, the combination of all other corrections gives an effect which is about 10% in the soft-p_{T} region and diminishes towards negative values at large p_{T}.

The transverse momentum of the $b\bar{b}$ system [Fig. 8(b)] is correlated to the one of $t\bar{t}$ system. The NLO_2 corrections to this observable behave in the same manner as those for the $p_{\mathrm{T},t\bar{t}}$ distributions, giving a -20% contribution around 400 GeV. The NLO_3 corrections grow monotonically from $+10\%$ (at low transverse momentum)

[2] In Ref. [40] the scale for the differential distributions is $\mu_0^{(\mathrm{d})}$, *i.e.* exactly twice the default scale used here.

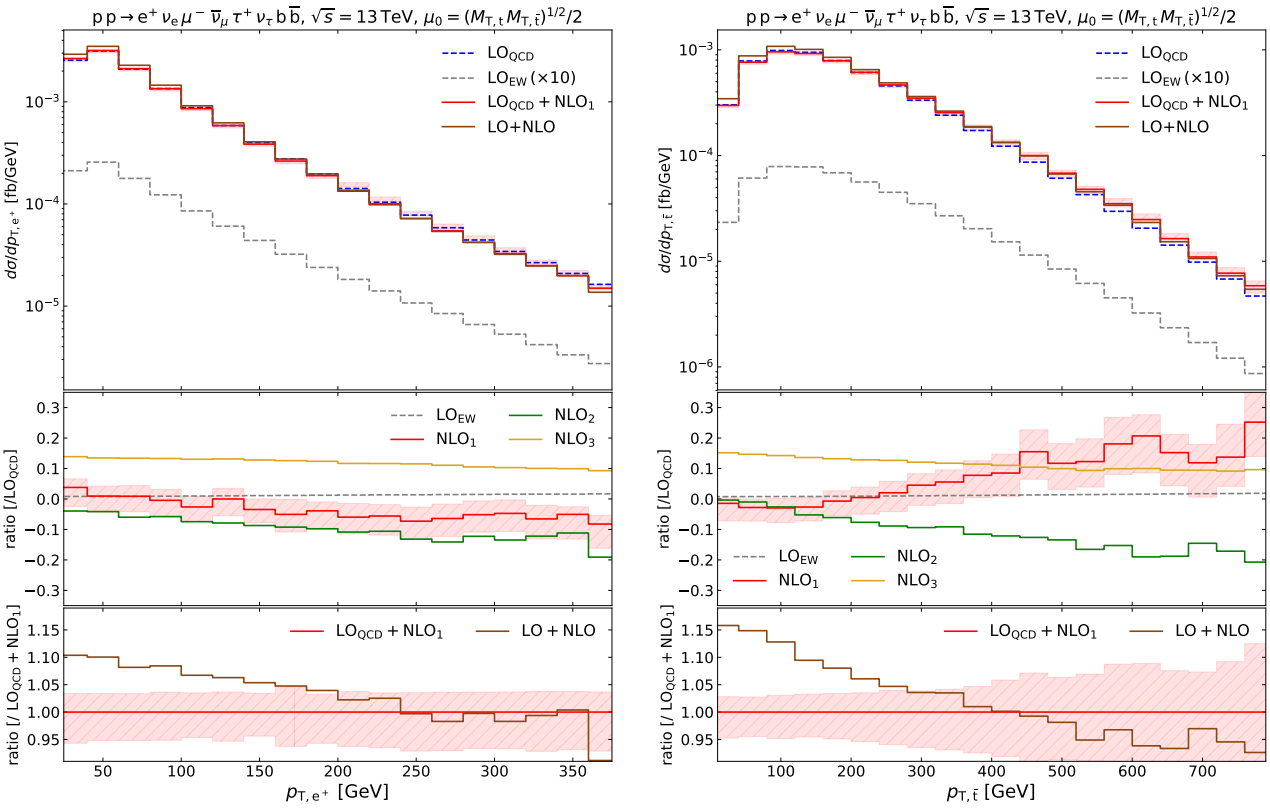

(a) Transverse momentum of the positron.

(b) Transverse momentum of the antitop quark.

Fig. 7. Distributions in the transverse momentum of the positron (left) and of the antitop quark (right). Top panel: differential cross-sections (in fb) for $\mathrm{LO_{QCD}}$, $\mathrm{LO_{EW}}$ (scaled by a factor 10), $\mathrm{LO_{QCD}} + \mathrm{NLO_1}$ and for the complete NLO, which is the sum of all LO cross-sections and all NLO corrections. Middle panel: ratio of the $\mathrm{LO_{EW}}$, $\mathrm{NLO_1}$, $\mathrm{NLO_2}$, and $\mathrm{NLO_3}$ corrections over the $\mathrm{LO_{QCD}}$ cross-section. Bottom panel: ratio of the $\mathrm{LO} + \mathrm{NLO}$ cross-section over the $\mathrm{LO_{QCD}} + \mathrm{NLO_1}$ one. Uncertainties from 7-point scale variations are shown in all panels for the $\mathrm{LO_{QCD}} + \mathrm{NLO_1}$ predictions.

to +30% (around 400 GeV). In the soft part of the spectrum ($p_{\mathrm{T,b\bar{b}}} < 150\,\mathrm{GeV}$), the $\mathrm{NLO_1}$ corrections are rather flat, while in the large-p_{T} region they grow positive and become very large, similarly to the $p_{\mathrm{T,t\bar{t}}}$ distribution. The overall NLO corrections are very small below 150 GeV due to mutual cancellations among the three contributions, while at larger transverse momenta the corrections are dominated by the $\mathrm{NLO_1}$ contribution. Furthermore, relatively to the $\mathrm{LO_{QCD}} + \mathrm{NLO_1}$ distribution, the combined NLO corrections give a flat and positive effect between 7% and 8% in the whole analyzed spectrum.

In all analyzed transverse-momentum distributions of Figures 7–8, the $\mathrm{LO_{EW}}$ contribution increases monotonically (relatively to the $\mathrm{LO_{QCD}}$ one) but never exceeds 3% of the $\mathrm{LO_{QCD}}$ cross-section.

In Fig. 9(a), we display the distribution in the invariant mass of the antitop quark, which in our setup can be reconstructed from the Monte Carlo truth. The lineshape is dominated by the Breit-Wigner distribution of the leptonic decay of the antitop quark. The $\mathrm{NLO_1}$ corrections are negative at the peak while below the pole mass they give a very large enhancement to the LO result. Such a radiative tail, coming from unclustered real radiation, is also present, though less sizeable, in the NLO EW corrections (unclustered photons). At values larger than the top-quark mass, the distribution receives an increasingly positive contribution from $\mathrm{NLO_1}$ corrections, while the $\mathrm{NLO_2}$ ones give an almost flat correction of −10% to the $\mathrm{LO_{QCD}}$ cross-section. The $\mathrm{LO_{EW}}$ contribution shows a slightly wider distribution than the $\mathrm{LO_{QCD}}$ one. This could be attributed to the relatively larger contribution of non-resonant background diagrams in the $\mathrm{LO_{EW}}$ contribution. Nonetheless, the impact of this difference on the full distribution is almost invisible owing to the very small size of the $\mathrm{LO_{EW}}$ contribution. The $\mathrm{NLO_3}$ corrections behave differently from the $\mathrm{NLO_1}$ ones, giving a rather flat enhancement of the fiducial LO cross-section, which is minimal around the peak (+11% at m_{t}) and mildly increases towards the tails (+20% at 200 GeV, +30% at 150 GeV). This is due to the very large contribution of the u(c)g partonic channel, which has a light d(s) in the final state that cannot come from the radiative decay of the top or of the antitop quark (differently from final-state gluons). As can be seen in the bottom panel of Fig. 9(a), the total $\mathrm{LO} + \mathrm{NLO}$ result is 12% higher than the $\mathrm{LO_{QCD}} + \mathrm{NLO_1}$ one below the top-quark mass. This enhancement is smaller at (4%) and above (7%) the top mass.

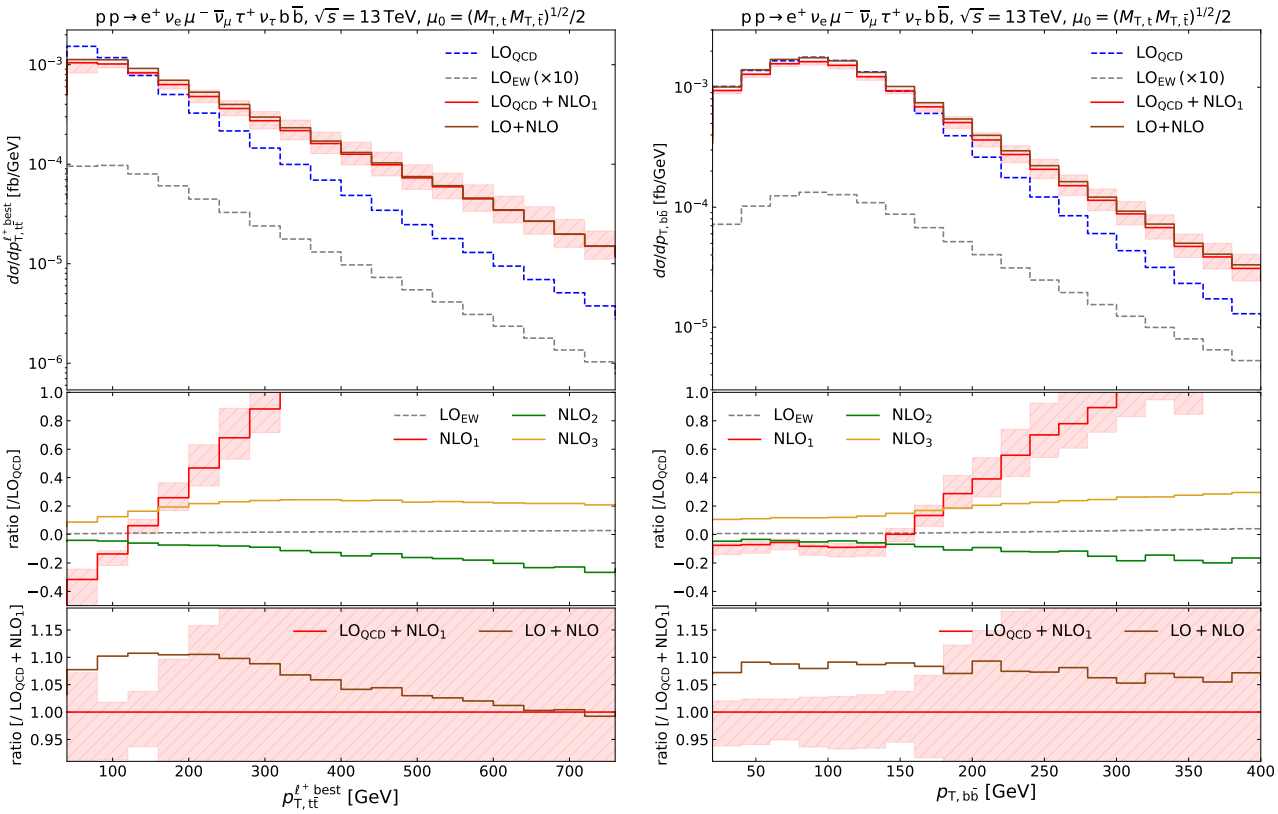

(a) Transverse momentum of the $t\bar{t}$ system.

(b) Transverse momentum of the $b\bar{b}$ system.

Fig. 8. Distributions in the transverse momentum of the reconstructed $t\bar{t}$ system (left) and of the $b\bar{b}$ system (right). Same structure as Fig. 7.

Another variable that is often investigated in LHC analyses is H_T, whose definition is given in Eq. (9). The LO and NLO distributions in this observable are shown in Fig. 9(b). As in the transverse-momentum distributions studied above, the NLO_2 radiative corrections decrease monotonically towards large values of H_T (about -20% for $H_T \approx 1.2\,\text{TeV}$). The LO_{EW} contribution grows to 5% of the LO_{QCD} cross-section at 1.5 TeV, where the NLO cross-section is two orders of magnitude lower than its value at the maximum of the distribution. The NLO_3 corrections are rather flat and enhance the LO_{QCD} result between 10% and 15%. The NLO_1 corrections are characterized by a non-flat shape that is increasing for $H_T < 800\,\text{GeV}$ from -10% to $+25\%$ and decreasing in the rest of the considered spectrum. We further observe that the combination of the three NLO perturbative orders yields an almost vanishing correction in the soft region of the spectrum, while in the tail of the distribution the overall correction is dominated by the NLO_2 contribution for our scale choice. In a similar fashion as in other transverse-momentum distributions, the ratio of the combined LO+NLO result over the $LO_{QCD}+NLO_1$ decreases monotonically from 1.15 to 0.95 in the analyzed range.

In Fig. 10 we study more invariant-mass distributions. The distribution in the invariant mass of the two-b-jet system [Fig. 10(a)] is characterized by rather flat QCD corrections (NLO_1 and NLO_3). The NLO_3 corrections enhance the LO_{QCD} cross-section by 11% to 14% everywhere in the analyzed invariant-mass range. The NLO_2 contribution has a similar behaviour as the one found for the previous variables, growing negative towards the tail of the distribution.

The distribution in the invariant mass of the three-charged-lepton system is considered in Fig. 10(b). The behaviour of the NLO_2 and NLO_3 corrections follows closely the one for the $b\bar{b}$ system, apart from a less steep decrease of the EW corrections towards large invariant masses. These corrections are at the -10% level for masses larger than 500 GeV. The NLO_1 corrections vary by hardly more than 10% in the studied range.

As shown in the bottom panels of Fig. 10, both for the $b\bar{b}$ system and for the three-charged-lepton system, the inclusion of NLO_2 and NLO_3 corrections (as well as of LO_{EW}, though hardly visible) gives a non-flat correction to the NLO QCD invariant-mass distributions, decreasing monotonically from $+12\%$ to zero in the considered spectra.

After presenting transverse-momentum and invariant-mass distributions, we switch to some relevant angular variables. In Fig. 11(a) and Fig. 11(b) we display the distributions in the rapidity of the muon and of the antitop quark, respectively. Since these two variables are correlated (the dominant resonant structure involves the decay $\bar{t} \to \bar{b}\mu^-\bar{\nu}_\mu$), the muon rapidity, which is precisely mea-

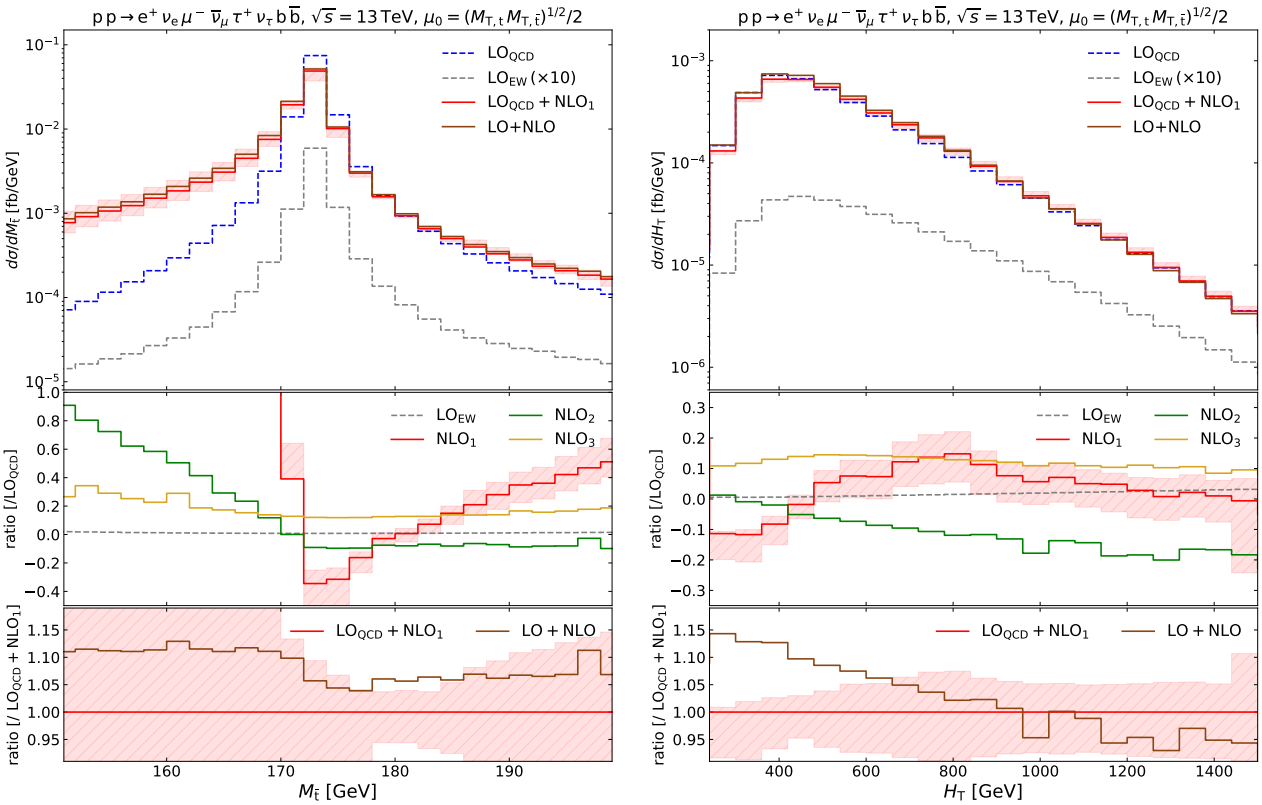

(a) Invariant mass of the antitop quark.

(b) H_{T} variable.

Fig. 9. Distributions in the invariant mass of the antitop quark (left) and in the H_{T} variable (right). Same structure as Fig. 7.

surable at the LHC, represents a suitable proxy for the rapidity of the corresponding antitop quark (which can only be reconstructed from Monte Carlo truth). Note that the muon rapidity is sharply cut at ± 2.5 by fiducial selections, while this is not the case for the antitop quark. However, thanks to the rapidity cut applied to b jets, the cross-section is strongly suppressed for $|y_{\bar{\mathrm{t}}}| > 2.5$. Both the muon and the antitop quark are produced preferably in the central region. The NLO_2 corrections are rather flat, giving between -4% and -8% decrease to the LO cross-section. The relative NLO_1 corrections to the muon-rapidity distribution are characterized by a large variation (about 35%) in the available range. Relative to $\mathrm{LO}_{\mathrm{QCD}}$, the differential NLO_3 corrections have a similar shape as the NLO_1 ones, giving in the whole rapidity range a positive correction (8% in the forward regions, 16% in the central region). Almost identical results are found in the rapidity distribution of the antitop quark. Owing to the NLO_3 corrections, the ratio between the complete NLO prediction and the $\mathrm{LO}_{\mathrm{QCD}}+\mathrm{NLO}_1$ one has a maximum of 1.11 in the central region and diminishes towards forward regions (close to unity). This holds both for the muon and for the antitop-quark rapidity spectra.

In Fig. 12(a) we consider the distribution in the azimuthal separation between the positron and the muon. The two charged leptons tend to be produced in opposite directions both at LO and at NLO, but the inclusion of radiative corrections enhances the fraction of events with small azimuthal separations. The NLO_2 corrections are negative and roughly constant (-5% to -7%) over the full angular range, while the NLO_3 contribution decreases monotonically from $+18\%$ to $+11\%$ relatively to the $\mathrm{LO}_{\mathrm{QCD}}$ result. As already observed in Ref. [40], the NLO_1 correction to the LO QCD cross-section decreases with an almost constant negative slope over the full range. The overall NLO corrections to the $\mathrm{LO}_{\mathrm{QCD}}$ cross-section are positive everywhere except in the vicinity of the peak at $\Delta\phi_{\mathrm{e}^+\mu^-} = \pi$. Relative to the $\mathrm{LO}_{\mathrm{QCD}} + \mathrm{NLO}_1$ prediction, the combination of NLO_2 and NLO_3 corrections gives a pretty flat enhancement (1.11 at $\Delta\phi_{\mathrm{e}^+\mu^-} = 0$, 1.06 at $\Delta\phi_{\mathrm{e}^+\mu^-} = \pi$).

As a last differential result, we present in Fig. 12(b) the distribution in the R distance between the two b jets [see Eq. (8) for its definition]. This distribution is characterized by an absolute maximum around $\Delta R_{\mathrm{b}\bar{\mathrm{b}}} \approx \pi$. The negative NLO_2 corrections diminish monotonically over the analyzed spectrum. At large distance ($\Delta R_{\mathrm{b}\bar{\mathrm{b}}} > 5$) they give a contribution of -15%. The positive NLO_3 corrections diminish from $+15\%$ at $\Delta R_{\mathrm{b}\bar{\mathrm{b}}} \approx 0$ to $+12\%$ at $\Delta R_{\mathrm{b}\bar{\mathrm{b}}} \approx \pi$ and then increase again. The NLO_1 ones show a similar behaviour, however, with larger slopes. The combined NLO_2 and NLO_3 corrections enhance the $\mathrm{LO}_{\mathrm{QCD}}+\mathrm{NLO}_1$ prediction between 6% and 11%, similarly to the case of the azimuthal distance shown in Fig. 12(a), but with a somewhat different shape.

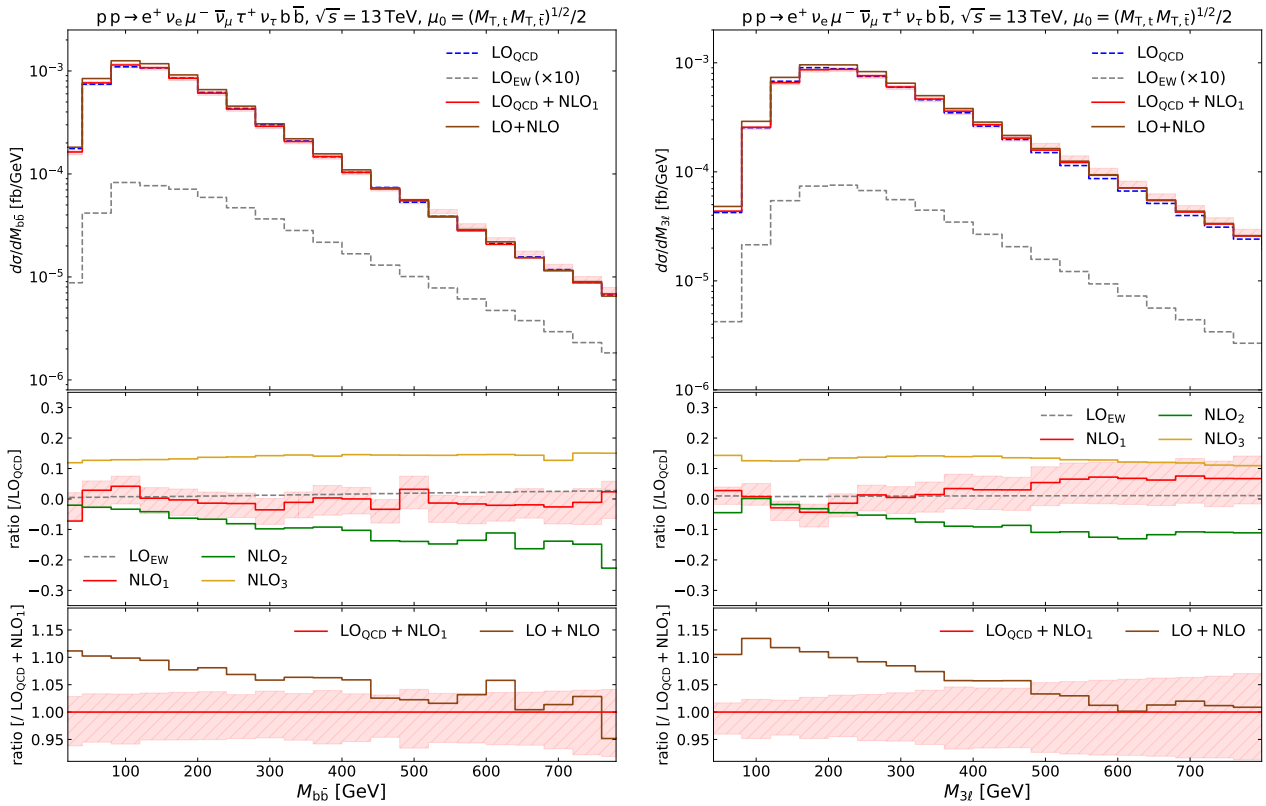

(a) Invariant mass of the $b\bar{b}$ system.

(b) Invariant mass of the three-charged-lepton system.

Fig. 10. Distributions in the invariant mass of the $b\bar{b}$ system (left) and of the three-charged-lepton system (right). Same structure as Fig. 7.

The results for the differential distributions presented in Figs. 7–12 show that in many kinematic regions the NLO_2 and NLO_3 corrections give an enhancement at the level of 10% to the $LO_{QCD} + NLO_1$ result that is larger than the QCD scale uncertainties at the same perturbative order. This concerns in particular the soft- and moderate-p_T, the low-mass and the central-rapidity regions, which are also the statistically most-populated ones. This reinforces that including formally subleading corrections (NLO_2, NLO_3) is necessary to give a more realistic description of total and differential $t\bar{t}W$ cross-sections.

4 Conclusions

In this work we have presented the NLO corrections to the off-shell production of $t\bar{t}W^+$ at the LHC in the three-charged-lepton channel. These include the next-to-leading-order (NLO) QCD corrections to the QCD (NLO_1) and to the electroweak leading order (NLO_3), as well as the NLO electroweak corrections to the QCD leading order (NLO_2). It is the first time that the NLO_2 and NLO_3 radiative corrections are computed with full off-shell dependence for a physical final state, accounting for all non-resonant, interference, and spin-correlation effects.

Both integrated and differential cross-sections have been presented and discussed in a realistic fiducial region, keeping in mind the limited statistics of the LHC data and relating the off-shell description of the process to the inclusive predictions that are available in the literature.

The NLO_2 and NLO_3 corrections give a -5.5% and a $+13\%$ contribution, respectively, to the LO cross-section, almost independently of the choice of the factorization and renormalization scales. The sizeable impact of NLO_2 and NLO_3 corrections makes it essential to combine them with the NLO_1 ones, in order to arrive at reliable predictions.

The theory uncertainties from 7-point scale variations are driven by the NLO_1 corrections, which are the only corrections which feature a NLO-like scale dependence. Their inclusion reduces the scale uncertainty of the LO cross-section from 20% to 5%.

The investigation of differential distributions reveals a more involved interplay among the various perturbative orders compared with the integrated results. The NLO_2 corrections drop by up to -20% in most of the transverse-momentum and invariant-mass distributions, showing the typical behaviour of EW corrections with large Sudakov logarithms at high energies. They are rather flat for angular observables. The NLO_3 corrections give a positive enhancement between $+10\%$ and $+20\%$ (30% in some

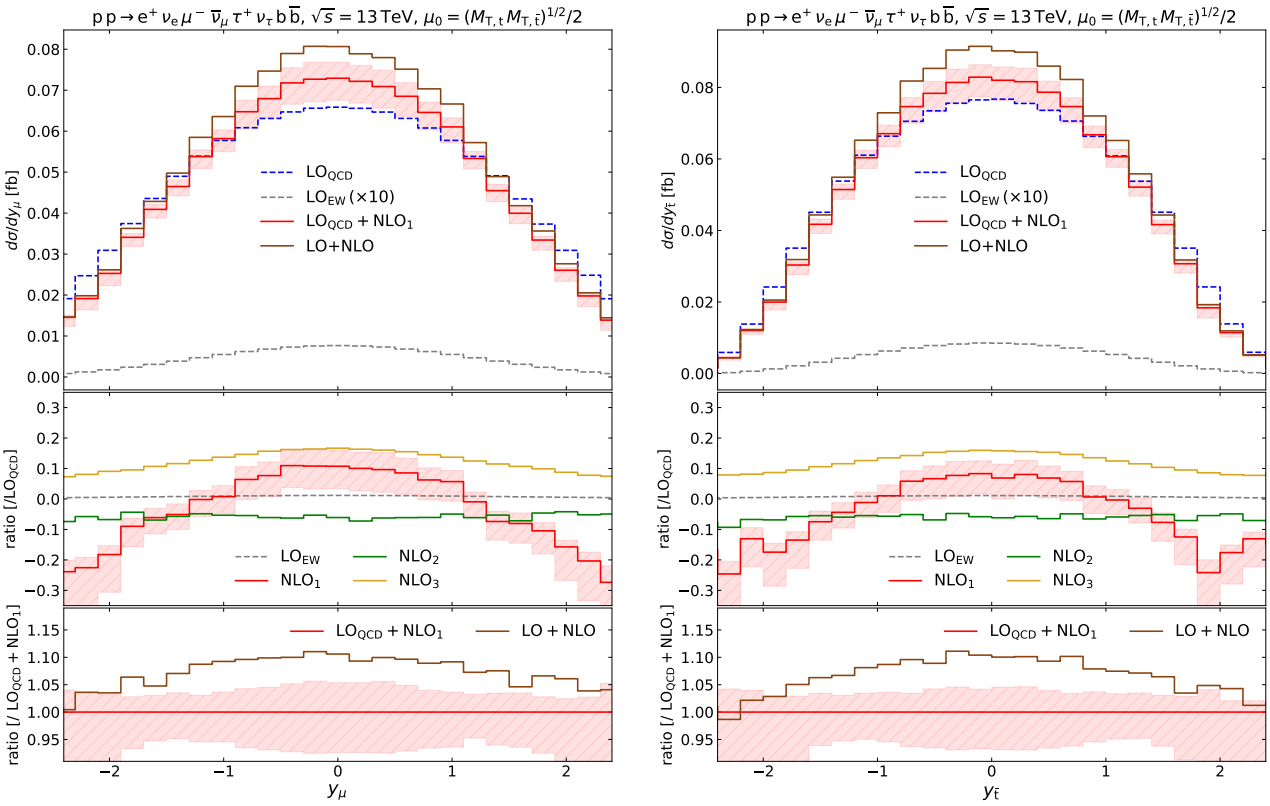

(a) Rapidity of the muon.

(b) Rapidity of the antitop quark.

Fig. 11. Distributions in the rapidity of the muon (left) and of the antitop quark (right). Same structure as Fig. 7.

cases) to the LO cross-section in all analyzed distributions, They are dominated by the ug partonic channel (formally belonging to QCD real corrections to LO EW) that embeds tW scattering. The NLO_1 corrections, which have already been presented in the literature, show quite variable patterns in the various differential K-factors.

We stress that all three NLO contributions usually give non-flat corrections to the LO distributions, also to the angular ones. This indicates that rescaling QCD results (either LO or NLO accurate) by flat K-factors could result in a bad description of some LHC observables.

In the light of an improved experimental description of the $\mathrm{t\bar{t}W}$ process, the inclusion of decay and off-shell effects is mandatory. Although for sufficiently inclusive observables the full computation is well approximated by on-shell calculations, the inclusion of off-shell effects in the modeling of $\mathrm{t\bar{t}W}$ production is definitely needed when studying the tails of transverse-momentum and invariant-mass observables.

Acknowledgements

We thank Mathieu Pellen for useful discussions on photon-induced electroweak real corrections, Timo Schmidt for performing checks with MoCaNLO, and Jean-Nicolas Lang and Sandro Uccirati for maintaining Recola. This work is supported by the German Federal Ministry for Education and Research (BMBF) under contract no. 05H18WWCA1.

References

1. J. A. Dror, M. Farina, E. Salvioni, J. Serra, Strong tW Scattering at the LHC, JHEP 01 (2016) 071. `arXiv:1511.03674`, `doi:10.1007/JHEP01(2016)071`.
2. A. Buckley, C. Englert, J. Ferrando, D. J. Miller, L. Moore, M. Russell, C. D. White, Constraining top quark effective theory in the LHC Run II era, JHEP 04 (2016) 015. `arXiv:1512.03360`, `doi:10.1007/JHEP04(2016)015`.
3. O. Bessidskaia Bylund, F. Maltoni, I. Tsinikos, E. Vryonidou, C. Zhang, Probing top quark neutral couplings in the Standard Model Effective Field Theory at NLO in QCD, JHEP 05 (2016) 052. `arXiv:1601.08193`, `doi:10.1007/JHEP05(2016)052`.
4. F. Maltoni, M. Mangano, I. Tsinikos, M. Zaro, Top-quark charge asymmetry and polarization in $t\bar{t}W^{\pm}$ production at the LHC, Phys. Lett. B 736 (2014) 252–260. `arXiv:1406.3262`, `doi:10.1016/j.physletb.2014.07.033`.
5. G. Bevilacqua, H.-Y. Bi, H. B. Hartanto, M. Kraus, J. Nasufi, M. Worek, NLO QCD corrections to off-

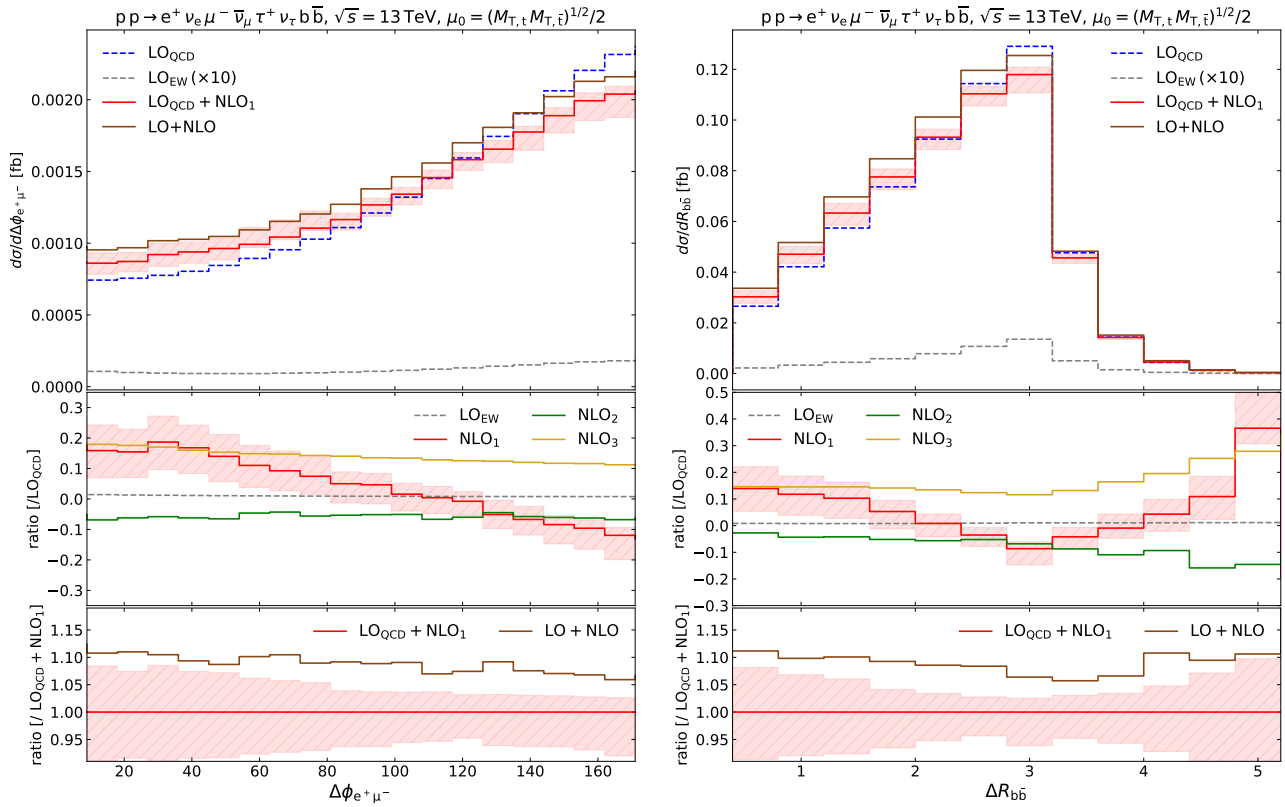

(a) Azimuthal angle between the positron and the muon.

(b) R distance between the two b jets.

Fig. 12. Distributions in the azimuthal difference between the positron and the muon (left) and in the azimuthal-angle–rapidity distance between the b jet and the $\bar{b}$ jet (right). Same structure as Fig. 7.

shell $t\bar{t}W^{\pm}$ production at the LHC: Correlations and Asymmetries (12 2020). arXiv:2012.01363.

6. R. Barnett, J. F. Gunion, H. E. Haber, Discovering supersymmetry with like sign dileptons, Phys. Lett. B 315 (1993) 349–354. arXiv:hep-ph/9306204, doi:10.1016/0370-2693(93)91623-U.
7. M. Guchait, D. Roy, Like sign dilepton signature for gluino production at CERN LHC including top quark and Higgs boson effects, Phys. Rev. D 52 (1995) 133–141. arXiv:hep-ph/9412329, doi:10.1103/PhysRevD.52.133.
8. H. Baer, C.-h. Chen, F. Paige, X. Tata, Signals for minimal supergravity at the CERN large hadron collider. 2: Multi-lepton channels, Phys. Rev. D 53 (1996) 6241–6264. arXiv:hep-ph/9512383, doi:10.1103/PhysRevD.53.6241.
9. R. Chivukula, E. H. Simmons, J. Terning, A heavy top quark and the $Zb\bar{b}$ vertex in non-commuting extended technicolor, Phys. Lett. B 331 (1994) 383–389. arXiv:hep-ph/9404209, doi:10.1016/0370-2693(94)91068-5.
10. J. Aguilar-Saavedra, R. Benbrik, S. Heinemeyer, M. Pérez-Victoria, Handbook of vectorlike quarks: Mixing and single production, Phys. Rev. D 88 (2013) 094010. arXiv:1306.0572, doi:10.1103/PhysRevD.88.094010.
11. F. M. L. Almeida Jr., Y. do Amaral Coutinho, J. A. Martins Simões, P. Queiroz Filho, C. Porto, Same-sign dileptons as a signature for heavy Majorana neutrinos in hadron hadron collisions, Phys. Lett. B 400 (1997) 331–334. arXiv:hep-ph/9703441, doi:10.1016/S0370-2693(97)00143-3.
12. J. Maalampi, N. Romanenko, Single production of doubly charged Higgs bosons at hadron colliders, Phys. Lett. B 532 (2002) 202–208. arXiv:hep-ph/0201196, doi:10.1016/S0370-2693(02)01549-6.
13. M. Perelstein, Little Higgs models and their phenomenology, Prog. Part. Nucl. Phys. 58 (2007) 247–291. arXiv:hep-ph/0512128, doi:10.1016/j.ppnp.2006.04.001.
14. R. Contino, G. Servant, Discovering the top partners at the LHC using same-sign dilepton final states, JHEP 06 (2008) 026. arXiv:0801.1679, doi:10.1088/1126-6708/2008/06/026.
15. F. Maltoni, D. Pagani, I. Tsinikos, Associated production of a top-quark pair with vector bosons at NLO in QCD: impact on $t\bar{t}H$ searches at the LHC, JHEP 02 (2016) 113. arXiv:1507.05640, doi:10.1007/JHEP02(2016)113.
16. G. Aad, et al., Measurement of the $t\bar{t}W$ and $t\bar{t}Z$ production cross sections in pp collisions at $\sqrt{s} = 8\,\mathrm{TeV}$ with the ATLAS detector, JHEP 11 (2015) 172. arXiv:1509.05276, doi:10.1007/

JHEP11(2015)172.

17. V. Khachatryan, et al., Observation of top quark pairs produced in association with a vector boson in pp collisions at $\sqrt{s} = 8\,\text{TeV}$, JHEP 01 (2016) 096. arXiv:1510.01131, doi:10.1007/JHEP01(2016)096.
18. M. Aaboud, et al., Measurement of the $t\bar{t}Z$ and $t\bar{t}W$ production cross sections in multilepton final states using $3.2\,\text{fb}^{-1}$ of pp collisions at $\sqrt{s} = 13\,\text{TeV}$ with the ATLAS detector, Eur. Phys. J. C77 (2017) 40. arXiv:1609.01599, doi:10.1140/epjc/s10052-016-4574-y.
19. A. M. Sirunyan, et al., Measurement of the cross section for top quark pair production in association with a W or Z boson in proton-proton collisions at $\sqrt{s} = 13\,\text{TeV}$, JHEP 08 (2018) 011. arXiv:1711.02547, doi:10.1007/JHEP08(2018)011.
20. M. Aaboud, et al., Measurement of the $t\bar{t}Z$ and $t\bar{t}W$ cross sections in proton-proton collisions at $\sqrt{s} = 13\,\text{TeV}$ with the ATLAS detector, Phys. Rev. D99 (2019) 072009. arXiv:1901.03584, doi:10.1103/PhysRevD.99.072009.
21. A. M. Sirunyan, et al., Measurement of top quark pair production in association with a Z boson in proton-proton collisions at $\sqrt{s} = 13\,\text{TeV}$, JHEP 03 (2020) 056. arXiv:1907.11270, doi:10.1007/JHEP03(2020)056.
22. M. Aaboud, et al., Observation of Higgs boson production in association with a top quark pair at the LHC with the ATLAS detector, Phys. Lett. B 784 (2018) 173–191. arXiv:1806.00425, doi:10.1016/j.physletb.2018.07.035.
23. A. M. Sirunyan, et al., Observation of $t\bar{t}H$ production, Phys. Rev. Lett. 120 (2018) 231801. arXiv:1804.02610, doi:10.1103/PhysRevLett.120.231801.
24. Analysis of $t\bar{t}H$ and $t\bar{t}W$ production in multilepton final states with the ATLAS detector, Tech. Rep. ATLAS-CONF-2019-045, CERN, Geneva (Oct 2019). URL http://cds.cern.ch/record/2693930
25. Search for Higgs boson production in association with top quarks in multilepton final states at $\sqrt{s} = 13\,\text{TeV}$, Tech. Rep. CMS-PAS-HIG-17-004, CERN, Geneva (2017). URL https://cds.cern.ch/record/2256103
26. J. M. Campbell, R. K. Ellis, $t\bar{t}W^{\pm}$ production and decay at NLO, JHEP 07 (2012) 052. arXiv:1204.5678, doi:10.1007/JHEP07(2012)052.
27. M. V. Garzelli, A. Kardos, C. G. Papadopoulos, Z. Trócsányi, $t\bar{t}W^{\pm}$ and $t\bar{t}Z$ Hadroproduction at NLO accuracy in QCD with Parton Shower and Hadronization effects, JHEP 11 (2012) 056. arXiv:1208.2665, doi:10.1007/JHEP11(2012)056.
28. S. Frixione, V. Hirschi, D. Pagani, H. S. Shao, M. Zaro, Electroweak and QCD corrections to top-pair hadroproduction in association with heavy bosons, JHEP 06 (2015) 184. arXiv:1504.03446, doi:10.1007/JHEP06(2015)184.
29. R. Frederix, D. Pagani, M. Zaro, Large NLO corrections in $t\bar{t}W^{\pm}$ and $t\bar{t}t\bar{t}$ hadroproduction from supposedly subleading EW contributions, JHEP 02 (2018) 031. arXiv:1711.02116, doi:10.1007/JHEP02(2018)031.
30. R. Frederix, S. Frixione, V. Hirschi, D. Pagani, H.-S. Shao, M. Zaro, The automation of next-to-leading order electroweak calculations, JHEP 07 (2018) 185. arXiv:1804.10017, doi:10.1007/JHEP07(2018)185.
31. H. T. Li, C. S. Li, S. A. Li, Renormalization group improved predictions for $t\bar{t}W^{\pm}$ production at hadron colliders, Phys. Rev. D 90 (2014) 094009. arXiv:1409.1460, doi:10.1103/PhysRevD.90.094009.
32. A. Broggio, A. Ferroglia, G. Ossola, B. D. Pecjak, Associated production of a top pair and a W boson at next-to-next-to-leading logarithmic accuracy, JHEP 09 (2016) 089. arXiv:1607.05303, doi:10.1007/JHEP09(2016)089.
33. A. Kulesza, L. Motyka, D. Schwartländer, T. Stebel, V. Theeuwes, Associated production of a top quark pair with a heavy electroweak gauge boson at NLO+NNLL accuracy, Eur. Phys. J. C 79 (2019) 249. arXiv:1812.08622, doi:10.1140/epjc/s10052-019-6746-z.
34. A. Broggio, A. Ferroglia, R. Frederix, D. Pagani, B. D. Pecjak, I. Tsinikos, Top-quark pair hadroproduction in association with a heavy boson at NLO+NNLL including EW corrections, JHEP 08 (2019) 039. arXiv:1907.04343, doi:10.1007/JHEP08(2019)039.
35. A. Kulesza, L. Motyka, D. Schwartländer, T. Stebel, V. Theeuwes, Associated top quark pair production with a heavy boson: differential cross sections at NLO+NNLL accuracy, Eur. Phys. J. C 80 (2020) 428. arXiv:2001.03031, doi:10.1140/epjc/s10052-020-7987-6.
36. S. von Buddenbrock, R. Ruiz, B. Mellado, Anatomy of inclusive $t\bar{t}W$ production at hadron colliders, Phys. Lett. B 811 (2020) 135964. arXiv:2009.00032, doi:10.1016/j.physletb.2020.135964.
37. R. Frederix, I. Tsinikos, Subleading EW corrections and spin-correlation effects in $t\bar{t}W$ multi-lepton signatures, Eur. Phys. J. C 80 (2020) 803. arXiv:2004.09552, doi:10.1140/epjc/s10052-020-8388-6.
38. F. F. Cordero, M. Kraus, L. Reina, Top-quark pair production in association with a $W^{\pm}$ gauge boson in the POWHEG-BOX (1 2021). arXiv:2101.11808.
39. G. Bevilacqua, H.-Y. Bi, H. B. Hartanto, M. Kraus, M. Worek, The simplest of them all: $t\bar{t}W^{\pm}$ at NLO accuracy in QCD, JHEP 08 (2020) 043. arXiv:2005.09427, doi:10.1007/JHEP08(2020)043.
40. A. Denner, G. Pelliccioli, NLO QCD corrections to off-shell $\mathrm{t\bar{t}W^{+}}$ production at the LHC, JHEP 11 (2020) 069. arXiv:2007.12089, doi:10.1007/JHEP11(2020)069.
41. S. Actis, A. Denner, L. Hofer, A. Scharf, S. Uccirati, Recursive generation of one-loop amplitudes in the Standard Model, JHEP 04 (2013) 037. arXiv:1211.6316, doi:10.1007/JHEP04(2013)037.
42. S. Actis, A. Denner, L. Hofer, J.-N. Lang, A. Scharf, S. Uccirati, RECOLA: REcursive Computation of One-Loop Amplitudes, Comput. Phys. Commun. 214 (2017) 140–173. arXiv:1605.01090, doi:10.1016/

j.cpc.2017.01.004.

43. A. Denner, S. Dittmaier, L. Hofer, COLLIER: a fortran-based Complex One-Loop LIbrary in Extended Regularizations, Comput. Phys. Commun. 212 (2017) 220–238. arXiv:1604.06792, doi:10.1016/j.cpc.2016.10.013.
44. A. Denner, M. Pellen, NLO electroweak corrections to off-shell top-antitop production with leptonic decays at the LHC, JHEP 08 (2016) 155. arXiv:1607.05571, doi:10.1007/JHEP08(2016)155.
45. A. Denner, J.-N. Lang, M. Pellen, S. Uccirati, Higgs production in association with off-shell top-antitop pairs at NLO EW and QCD at the LHC, JHEP 02 (2017) 053. arXiv:1612.07138, doi:10.1007/JHEP02(2017)053.
46. S. Catani, M. Seymour, A general algorithm for calculating jet cross-sections in NLO QCD, Nucl. Phys. B 485 (1997) 291–419, [Erratum: Nucl. Phys. B **510** (1998) 503–504]. arXiv:hep-ph/9605323, doi:10.1016/S0550-3213(96)00589-5.
47. S. Dittmaier, A general approach to photon radiation off fermions, Nucl. Phys. B 565 (2000) 69–122. arXiv:hep-ph/9904440, doi:10.1016/S0550-3213(99)00563-5.
48. S. Catani, S. Dittmaier, M. H. Seymour, Z. Trócsányi, The dipole formalism for next-to-leading order QCD calculations with massive partons, Nucl. Phys. B 627 (2002) 189–265. arXiv:hep-ph/0201036, doi:10.1016/S0550-3213(02)00098-6.
49. M. Tanabashi, et al., Review of Particle Physics, Phys. Rev. D 98 (2018) 030001. doi:10.1103/PhysRevD.98.030001.
50. D. Yu. Bardin, A. Leike, T. Riemann, M. Sachwitz, Energy-dependent width effects in e^+e^- annihilation near the Z-boson pole, Phys. Lett. B206 (1988) 539–542. doi:10.1016/0370-2693(88)91627-9.
51. M. Jeżabek, J. H. Kühn, QCD Corrections to Semileptonic Decays of Heavy Quarks, Nucl. Phys. B314 (1989) 1–6. doi:10.1016/0550-3213(89)90108-9.
52. L. Basso, S. Dittmaier, A. Huss, L. Oggero, Techniques for the treatment of IR divergences in decay processes at NLO and application to the top-quark decay, Eur. Phys. J. C76 (2016) 56. arXiv:1507.04676, doi:10.1140/epjc/s10052-016-3878-2.
53. A. Denner, S. Dittmaier, M. Roth, D. Wackeroth, Electroweak radiative corrections to $e^+e^- \to WW \to 4$ fermions in double pole approximation: The RACOONWW approach, Nucl. Phys. B587 (2000) 67–117. arXiv:hep-ph/0006307, doi:10.1016/S0550-3213(00)00511-3.
54. A. Denner, S. Dittmaier, M. Roth, D. Wackeroth, Predictions for all processes $e^+e^- \to 4\,\text{fermions} + \gamma$, Nucl. Phys. B560 (1999) 33–65. arXiv:hep-ph/9904472, doi:10.1016/S0550-3213(99)00437-X.
55. A. Denner, S. Dittmaier, M. Roth, L. H. Wieders, Electroweak corrections to charged-current $e^+e^- \to 4$ fermion processes: Technical details and further results, Nucl. Phys. B724 (2005) 247–294, [Erratum: Nucl. Phys. B **854** (2012) 504]. arXiv:hep-ph/0505042, doi:10.1016/j.nuclphysb.2011.09.001,10.1016/j.nuclphysb.2005.06.033.
56. A. Denner, S. Dittmaier, The complex-mass scheme for perturbative calculations with unstable particles, Nucl. Phys. B Proc. Suppl. 160 (2006) 22–26. arXiv:hep-ph/0605312, doi:10.1016/j.nuclphysbps.2006.09.025.
57. V. Bertone, S. Carrazza, N. P. Hartland, J. Rojo, Illuminating the photon content of the proton within a global PDF analysis, SciPost Phys. 5 (2018) 008. arXiv:1712.07053, doi:10.21468/SciPostPhys.5.1.008.
58. A. Buckley, J. Ferrando, S. Lloyd, K. Nordström, B. Page, M. Rüfenacht, M. Schönherr, G. Watt, LHAPDF6: parton density access in the LHC precision era, Eur. Phys. J. C 75 (2015) 132. arXiv:1412.7420, doi:10.1140/epjc/s10052-015-3318-8.
59. M. Cacciari, G. P. Salam, G. Soyez, The anti-k_t jet clustering algorithm, JHEP 04 (2008) 063. arXiv:0802.1189, doi:10.1088/1126-6708/2008/04/063.
60. A. Denner, S. Pozzorini, One loop leading logarithms in electroweak radiative corrections. 1. Results, Eur. Phys. J. C 18 (2001) 461–480. arXiv:hep-ph/0010201, doi:10.1007/s100520100551.